

Image reconstruction through metamorphosis

Barbara Gris ^{*} Chong Chen [†] Ozan Öktem [‡]

Abstract

This article adapts the framework of metamorphosis to solve inverse problems in imaging that includes joint reconstruction and image registration. The deformations in question have two components, one that is a geometric deformation moving intensities and the other a deformation of intensity values itself, which, e.g., allows for appearance of a new structure. The idea developed here is to reconstruct an image from noisy and indirect observations by registering, via metamorphosis, a template to the observed data. Unlike a registration with only geometrical changes, this framework gives good results when intensities of the template are poorly chosen. We show that this method is a well-defined regularisation method (proving existence, stability and convergence) and present several numerical examples.

1 Introduction

In *shape based reconstruction* or *spatiotemporal image reconstruction*, a key difficulty is to match an image against an indirectly observed target (*indirect image registration*). This paper provides theory and algorithms for indirect image registration applicable to general inverse problems. Before proceeding, we give a brief overview of these notions along with a short survey of existing results.

Shape based reconstruction The goal is to recover shapes of interior sub-structures of an object whereas variations within these is of less importance. Examples of such imaging studies are nano-characterisation of specimens by means of electron microscopy or x-ray phase contrast imaging, e.g., nano-characterisation of materials by electron electron tomography (ET) primarily focuses on the morphology of sub-structures [5]. Another example is quantification of sub-resolution porosity in materials by means of x-ray phase contrast imaging.

^{*}LJLL - Laboratoire Jacques-Louis Lions, UPMC, Paris, France.

[†]LSEC, ICMSEC, Academy of Mathematics and Systems Science, Chinese Academy of Sciences, Beijing 100190, People's Republic of China

[‡]Department of Mathematics, KTH – Royal Institute of Technology, Stockholm, Sweden.

In these imaging applications it makes sense to account for qualitative prior shape information during the reconstruction. Enforcing an exact spatial match between a template and the reconstruction is often too strong since realistic shape information is almost always approximate, so the natural approach is to perform reconstruction assuming the structures are ‘shape wise similar’ to a template.

Spatiotemporal imaging Imaging an object that undergoes temporal variation leads to a spatiotemporal reconstruction problem where both the object and its time variation needs to be recovered from noisy time series of measured data. An important case is when the only time dependency is that of the object.

Spatiotemporal imaging occurs in medical imaging, see, e.g., [23] for a survey of organ motion models. It is particularly relevant for techniques like positron emission tomography (PET) and single photon emission computed tomography (SPECT), which are used for visualising the distribution of injected radiopharmaceuticals (activity map). The latter is an inherently dynamic quantity, e.g., anatomical structures undergo motion, like the motion of the heart and respiratory motion of the lungs and thoracic wall, during the data acquisition. Not accounting for organ motion is known to degrade the spatial localisation of the radiotracer, leading to spatially blurred images. Furthermore, even when organ motion can be neglected, there are other dynamic processes, such as the uptake and wash-out of radiotracers from body organs. Visualising such kinetics of the radiotracers can actually be a goal in itself, as in pre-clinical imaging studies related to drug discovery/development. The term ‘dynamic’ in PET and SPECT imaging often refers to such temporal variation due to radiotracers kinetics rather than organ movement [13].

To exemplify the above mentioned issues, consider SPECT based cardiac perfusion studies and ^{18}F -FDG-PET imaging of lung nodules/tumours. The former needs to account for the beating heart and the latter for respiratory motion of the lungs and thoracic wall. Studies show a maximal displacement of 23 mm (average 15–20 mm) due to respiratory motion [21] and 42 mm (average 8–23 mm) due to cardiac motion in thoracic PET [25].

Indirect image registration (matching) In image registration the aim is to deform a template image so that it matches a target image, which becomes challenging when the template is allowed to undergo non-rigid deformations.

A well developed framework is diffeomorphic image registration where the image registration is recast as the problem of finding a suitable diffeomorphism that deforms the template into the target image [26, 2]. The underlying assumption is that the target image is contained in the orbit of

the template under the group action of diffeomorphisms. This can be stated in a very general setting where diffeomorphisms act on various structures, like landmark points, curves, surfaces, scalar images, or even vector/tensor valued images.

The registration problem becomes more challenging when the target is only known indirectly through measured data. This is referred to as *indirect image registration*, see [19] for using small diffeomorphic deformations and [9, 14] for adapting the large deformation diffeomorphic metric mapping (LDDMM) framework to indirect image registration.

2 Overview of paper and specific contributions

The paper adapts the metamorphosis framework [24] to the indirect image registration setting. Metamorphosis is an extension of the LDDMM framework (diffeomorphometry) [26, 16] where not only the geometry of the template, but also the grey-scale values undergo diffeomorphic changes.

We start by recalling necessary theory from LDDMM-based indirect registration (section 3). Using the notions from section 3, we adapt the metamorphosis framework to the indirect setting (section 4). We show how this framework allows to define a regularization method for inverse problems, satisfying properties of existence, stability and convergence (section 4.3). The numerical implementation is outlined in section 4.4. We present several numerical examples from 2D tomography, and in particular give a preliminary result for motion reconstruction when the acquisition is done at several time points. We also study the robustness of our methods with respects to the parameters (section 5).

3 Indirect diffeomorphic registration

3.1 Large diffeomorphic deformations

We recall here the notion of large diffeomorphic deformations defined by flows of time-varying vector fields, as formalized in [1].

Let $\Omega \subset \mathbb{R}^d$ be a fixed bounded domain and let $X := L^2(\Omega, \mathbb{R})$ represent grey scale images on Ω . Next, let V denote a fixed Hilbert space of vector fields on \mathbb{R}^d . We will assume $V \subset C_0^p(\Omega)$, i.e., the vector fields are supported on Ω and p times continuously differentiable. Finally, $L^1([0, 1], V)$ denotes the space of time-dependent V -vector fields that are integrable, i.e.,

$$\boldsymbol{\nu}(t, \cdot) \in V \quad \text{and} \quad t \mapsto \|\boldsymbol{\nu}(t, \cdot)\|_{C^p} \text{ is integrable on } [0, 1].$$

Furthermore, we will frequently make use of the following (semi) norm on

$$\|\boldsymbol{\nu}\|_p := \left(\int_0^1 \|\boldsymbol{\nu}(t, \cdot)\|_V^p dt \right)^{1/p}$$

where $\|\cdot\|_V$ is the naturally defined norm based upon the inner product of the Hilbert space V of vector fields.

The following proposition allows one to consider flows of elements in $L^1([0, 1], V)$ and ensures that these flows belong to $\text{Diff}_0^p(\Omega)$ (set of p -diffeomorphisms that are supported in $\Omega \subset \mathbb{R}^d$, and if Ω is unbounded, tend to zero towards infinity).

Proposition 1. *Let $\nu \in L^1([0, 1], V)$ and consider the ordinary differential equation (flow equation):*

$$\begin{cases} \frac{d}{dt}\phi(t, x) = \nu(t, \phi(t, x)) \\ \phi(0, x) = x \end{cases} \quad \text{for any } x \in \Omega \text{ and } t \in [0, 1]. \quad (1)$$

Then, (1) has a unique absolutely continuous solution $\phi(t, \cdot) \in \text{Diff}_0^p(\mathbb{R}^d)$.

The above result is proved in [1] and the unique solution of (1) is henceforth called the *flow of ν* . We also introduce to notation $\varphi_{s,t}^\nu: \mathbb{R}^d \rightarrow \mathbb{R}^d$ that refers to

$$\varphi_{s,t}^\nu := \phi(t, \cdot) \circ \phi(s, \cdot)^{-1} \quad \text{for } s, t \in [0, 1] \quad (2)$$

where $\phi: \Omega \rightarrow \mathbb{R}^d$ denotes the unique solution to (1).

As stated next, the set of diffeomorphisms that are given as flows forms a group that is a complete metric space [1].

Proposition 2. *Let $V \subset C_0^p(\Omega)$ ($p \geq 1$) be an admissible reproducing kernel Hilbert space (RKHS) and define*

$$G_V := \left\{ \phi: \mathbb{R}^d \rightarrow \mathbb{R}^d \mid \phi = \varphi_{0,1}^\nu \text{ for some } \nu \in L^2([0, 1], V) \right\}.$$

Then G_V forms a sub-group of $\text{Diff}_0^p(\mathbb{R}^d)$ that is a complete metric space under the metric

$$\begin{aligned} d_G(\phi_1, \phi_2) &:= \inf \left\{ \|\nu\|_1 : \nu \in L^1([0, 1], V) \text{ and } \phi_1 = \phi_2 \circ \varphi_{0,1}^\nu \right\} \\ &= \inf \left\{ \|\nu\|_2 : \nu \in L^1([0, 1], V) \text{ and } \phi_1 = \phi_2 \circ \varphi_{0,1}^\nu \right\}. \end{aligned}$$

The elements of G_V are called *large diffeomorphic deformations* and G_V acts on X via the *geometric group action* that is defined by the operator

$$\mathcal{W}: G_V \times X \rightarrow X \quad \text{where} \quad \mathcal{W}(\phi, I_0) := I_0 \circ \phi^{-1}. \quad (3)$$

We conclude by stating regularity properties of flows of velocity fields as well as the group action in (3), these will play an important role in what is to follow. The proof is given in [6].

Proposition 3. Assume $V \subset C_0^p(\Omega)$ ($p \geq 1$) is a fixed admissible Hilbert space of vector fields on Ω and $\{\nu^n\}_n \subset L^2([0, 1], V)$ a sequence that converges weakly to $\nu \in L^2([0, 1], V)$. Then, the following holds with $\varphi_t^n := \varphi_{0,t}^{\nu^n}$:

1. $(\varphi_t^n)^{-1}$ converges to $(\varphi_{0,t}^\nu)^{-1}$ uniformly w.r.t. $t \in [0, 1]$ and uniformly on compact subsets of $\Omega \subset \mathbb{R}^d$.
2. $\lim_{n \rightarrow \infty} \left\| \mathcal{W}(\varphi_t^n, I_0) - \mathcal{W}(\varphi_{0,t}^\nu, I_0) \right\|_X = 0$ for any $f \in X$.

3.2 Indirect image registration

Image registration (matching) refers to the task of deforming a given template image $I_0 \in X$ so that it matches a given target image $I^* \in X$.

The above task can also be stated in an *indirect* setting, which refers to the case when the template $I_0 \in X$ is to be registered against a target $I^* \in X$ that is only indirectly known through data $g \in Y$ where

$$g = \mathcal{A}(I^*) + e. \quad (4)$$

In the above, $\mathcal{A}: X \rightarrow Y$ (forward operator) is known and assumed to be differentiable and $e \in Y$ is a single sample of a Y -valued random element that denotes the measurement noise in the data.

A further development requires specifying what is meant by deforming a template image, and we will henceforth consider diffeomorphic (non-rigid) deformations, i.e., diffeomorphisms that deform images by acting on them through a group action.

LDDMM-based registration An example of using large diffeomorphic (non-rigid) deformations for image registration is to minimize the following functional:

$$G_V \ni \phi \mapsto \frac{\gamma}{2} d_G(\text{Id}, \phi)^2 + \left\| \mathcal{W}(\phi, I_0) - I^* \right\|_X^2 \quad \text{given } \gamma > 0.$$

If V is admissible, then minimizing the above functional on G_V amounts to minimizing the following functional on $L^2([0, 1], V)$ [26, Theorem 11.2 and Lemma 11.3]:

$$L^2([0, 1], V) \ni \nu \mapsto \frac{\gamma}{2} \|\nu\|_2^2 + \left\| \mathcal{W}(\varphi_{0,1}^\nu, I_0) - f \right\|_X^2 \quad \text{given } \gamma > 0.$$

Such a reformulation is advantageous since $L^2([0, 1], V)$ is a vector space, whereas G_V is not, so it is easier to minimize a functional over $L^2([0, 1], V)$ rather than over G_V .

The above can be extended to the indirect setting as shown in [9], which we henceforth refer to as *LDDMM-based indirect registration*. More precisely, the corresponding indirect registration problem can be addressed by

minimising the functional

$$L^2([0, 1], V) \ni \nu \mapsto \frac{\gamma}{2} \|\nu\|_2^2 + \mathcal{L}((\mathcal{A} \circ \mathcal{W})(\varphi_{0,t}^\nu, I_0), g).$$

Here, $\mathcal{L}: Y \times Y \rightarrow \mathbb{R}$ is typically given by an appropriate affine transform of the data negative log-likelihood [4], so minimizing $f \mapsto \mathcal{L}(\mathcal{A}(f), g)$ corresponds to seeking a maximum likelihood solution of (4).

An interpretation of the above is that the template image I_0 , which is assumed to be given a priori, acts as a *shape prior* when solving the inverse problem in (4) and $\gamma > 0$ is a regularization parameter that governs the influence of this shape priori against the need to fit measured data. This interpretation becomes more clear when one re-formulates LDDMM-based indirect registration as

$$\begin{cases} \min_{\nu \in L^2([0,1],V)} \left[\frac{\gamma}{2} \|\nu\|_2^2 + \mathcal{L}((\mathcal{A} \circ \mathcal{W})(\phi(1, \cdot), I_0), g) \right] \\ \frac{d}{dt} \phi(t, x) = \nu(t, \phi(t, x)) \quad (t, x) \in \Omega \times [0, 1], \\ \phi(0, x) = x \quad x \in \Omega. \end{cases} \quad (5)$$

4 Metamorphosis-based indirect registration

4.1 Motivation

As shown in [9], access to a template that can act as a shape prior can have profound effect in solving challenging inverse problem in imaging. As an example, tomographic imaging problems that are otherwise intractable (highly noisy and sparsely sampled data) can be successfully addressed using indirect registration even when using a template is far from the target image used for generating the data.

When template has correct topology and intensity levels, then LDDMM-based indirect registration with geometric group action is remarkably stable as shown in [9]. Using a geometric group action, however, makes it impossible to create or remove intensity, e.g., it is not possible to start out from a template with a single isolated structure and deform it to a image with two isolated structures. This severely limits the usefulness of LDDMM-based indirect registration, e.g., spatiotemporal images (moves) are likely to involve changes in both geometry (objects appear or disappear) and intensity. See fig. 1 for an example of how wrong intensity influences the registration.

As noted in [9], one approach is to replace the geometric group action with one that alters intensities, e.g., a mass preserving group action. Another is to keep the geometric group action, but replace LDDMM with a framework for diffeomorphic deformations that acts on both geometry and intensities, e.g., metamorphosis. This latter approach is the essence of metamorphosis-based indirect registration.

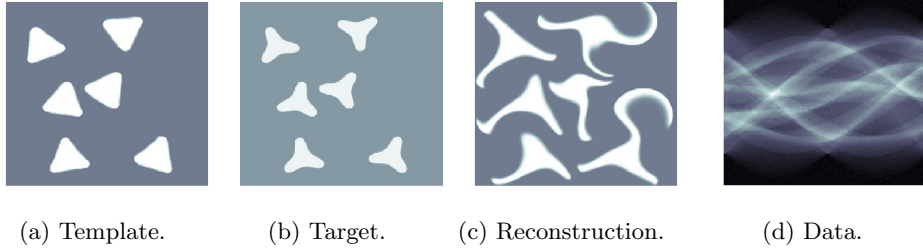


Figure 1: Reconstruction by LDDMM-based indirect registration (c) using a template (a) with a geometry that matches the target (b), but with incorrect background intensity values. Target is observed indirectly through tomographic data (d), which is 2D parallel beam Radon transform with 100 evenly distributed directions (see section 5.1 for details). The artefacts in the reconstruction are due to incorrect background intensity in template.

4.2 The metamorphosis framework

In metamorphosis diffeomorphisms are still generated by flows as in LDDMM, but the difference is that they now act with a geometric group action on *both* intensities and underlying points. As such, metamorphosis extends LDDMM. The abstract definition of a metamorphosis reads as follows.

Definition 1 (Metamorphosis [24]). *Let $V \subset C_0^p(\Omega)$ be an admissible Hilbert space and “ \cdot ” denotes some group action of G_V on X . A Metamorphosis is a curve $t \mapsto (\phi_t, J_t)$ in $G_V \times X$. The curve $t \mapsto f_t := \phi_t \cdot J_t$ is called the image part, $t \mapsto \phi_t$ is the deformation part, and $t \mapsto J_t$ is the template part.*

The image part represents the temporal evolution that is not related to intensity changes, i.e., evolution of underlying geometry, whereas the template part is the evolution of the intensity. Both evolutions, which are combined in metamorphosis, are driven by the same underlying flow of diffeomorphisms in G_V .

A important case is when the metamorphosis $t \mapsto (\phi_t, f_t)$ has a deformation part that solves the flow equation (1) and a template part is C^1 in time. More precisely, $L^2([0, 1], X)$ denotes the space of functions in X that are square integrable, i.e.,

$$\zeta(t, \cdot) \in X \quad \text{and} \quad t \mapsto \|\zeta(t, \cdot)\|_X \text{ is in } L^2([0, 1], \mathbb{R}).$$

The norm on $L^2([0, 1], X)$ is then

$$\|\zeta\|_2 := \left(\int_0^1 \|\zeta(t, \cdot)\|_X^2 dt \right)^{1/2}.$$

We will also use the notation

$$L^2([0, 1], V \times X) := L^2([0, 1], V) \times L^2([0, 1], X).$$

Bearing in mind the above notation, for given $(\boldsymbol{\nu}, \zeta) \in L^2([0, 1], V \times X)$ and $I_0 \in X$, define the curve $t \mapsto I_t^{\boldsymbol{\nu}, \zeta}$, which is absolutely continuous on $[0, 1]$, as the solution to

$$\begin{cases} \frac{d}{dt} I_t^{\boldsymbol{\nu}, \zeta}(x) = \zeta(t, \varphi_{0,t}^{\boldsymbol{\nu}}(x)) \\ I_0^{\boldsymbol{\nu}, \zeta}(x) = I_0(x) \end{cases} \quad \text{with } \varphi_{0,t}^{\boldsymbol{\nu}} \in G_V \text{ as in (2)}. \quad (6)$$

The metamorphosis can now be parametrised as $t \mapsto (\varphi_{0,t}^{\boldsymbol{\nu}}, I_t^{\boldsymbol{\nu}, \zeta})$.

Indirect registration The indirect registration problem in section 3.2 can be approached by metamorphosis instead of LDDMM. Similar to LDDMM-based indirect image registration in [9], we define *metamorphosis-based indirect image registration* as the minimization of the objective functional

$$\mathcal{J}_{\gamma, \tau}(\cdot; g): L^2([0, 1], V \times X) \rightarrow \mathbb{R}$$

defined as

$$\mathcal{J}_{\gamma, \tau}(\boldsymbol{\nu}, \zeta; g) := \frac{\gamma}{2} \|\boldsymbol{\nu}\|_2^2 + \frac{\tau}{2} \|\zeta\|_2^2 + \mathcal{L}\left(\mathcal{A}(\mathcal{W}(\varphi_{0,1}^{\boldsymbol{\nu}}, I_1^{\boldsymbol{\nu}, \zeta})), g\right) \quad (7)$$

for given regularization parameters $\gamma, \tau \geq 0$, measured data $g \in Y$, and initial template $I_0 \in X$ that sets the initial condition $I_0^{\boldsymbol{\nu}, \zeta}(x) := I_0(x)$.

Hence, performing metamorphosis-based indirect image registration of a template I_0 against a target indirectly observed through data g amounts to solving

$$(\widehat{\boldsymbol{\nu}}, \widehat{\zeta}) \in \arg \min_{(\boldsymbol{\nu}, \zeta)} \mathcal{J}_{\gamma, \tau}(\boldsymbol{\nu}, \zeta; g). \quad (8)$$

The above always has a solution assuming the data discrepancy and the forward operator fulfills some weak requirements (see proposition 4). From a solution we then obtain the following:

- *Initial template:* $I_0 \in X$ such that $I_0^{\boldsymbol{\nu}, \zeta} := I_0$.
- *Reconstruction:* Final registered template $f_1^{\widehat{\boldsymbol{\nu}}, \widehat{\zeta}} = \mathcal{W}(\varphi_{0,1}^{\widehat{\boldsymbol{\nu}}}, I_1^{\widehat{\boldsymbol{\nu}}, \widehat{\zeta}}) \in X$.
- *Image trajectory:* The evolution of both geometry and intensity of the template, given by $t \mapsto \mathcal{W}(\varphi_{0,t}^{\widehat{\boldsymbol{\nu}}}, I_t^{\widehat{\boldsymbol{\nu}}, \widehat{\zeta}})$.
- *Template trajectory:* The evolution of intensities of the template, i.e., the part that does not include evolution of geometry: $t \mapsto I_t^{\widehat{\boldsymbol{\nu}}, \widehat{\zeta}}$.
- *Deformation trajectory:* The geometric evolution of the template, i.e., the part that does not include evolution of intensity: $t \mapsto \mathcal{W}(\varphi_{0,t}^{\widehat{\boldsymbol{\nu}}}, I_0)$.

4.3 Regularising properties

In the following we prove several properties (existence, stability and convergence) of metamorphosis-based indirect image registration, which are necessary if the approach is to constitute a *well defined regularisation method* (notion defined in [12]). We set $X := L^2(\Omega, \mathbb{R})$ and Y a Hilbert space.

Proposition 4 (Existence). *Assume $\mathcal{A}: X \rightarrow Y$ is continuous and the data discrepancy $\mathcal{L}(\cdot, g): Y \rightarrow \mathbb{R}$ is weakly lower semi-continuous for any $g \in Y$. Then, $\mathcal{J}_{\gamma, \tau}(\cdot, g): L^2([0, 1], V \times X) \rightarrow \mathbb{R}$ defined through (6) and (7) has a minimizer in $L^2([0, 1], V \times X)$ for any $I_0 \in L^2(\Omega, \mathbb{R})$.*

Proof. We follow here the strategy to prove existence of minimal trajectories for metamorphosis (as in [8] for instance). One considers a minimizing sequence of $\mathcal{J}_{\gamma, \tau}(\cdot; g)$, i.e., a sequence that converges to the infimum of $\mathcal{J}_{\gamma, \tau}(\cdot; g)$ (such a sequence always exists). The idea is to prove that such a minimizing sequence has a sub-sequence that converges to a point in $L^2([0, 1], V \times X)$, i.e., the infimum is contained in $L^2([0, 1], V \times X)$ which proves existence of a minima.

Bearing in mind the above, we start by considering a minimizing sequence $\{(\boldsymbol{\nu}^n, \zeta^n)\}_n \subset L^2([0, 1], V \times X)$ to $\mathcal{J}_{\gamma, \tau}(\cdot; g)$, i.e.,

$$\lim_{n \rightarrow \infty} \mathcal{J}_{\gamma, \tau}(\boldsymbol{\nu}^n, \zeta^n; g) = \inf_{\boldsymbol{\nu}, \zeta} \mathcal{J}_{\gamma, \tau}(\boldsymbol{\nu}, \zeta; g).$$

Since $\{\boldsymbol{\nu}^n\}_n \subset L^2([0, 1], V)$ is bounded, it has a sub-sequence that converges to an element $\boldsymbol{\nu}^\infty \in L^2([0, 1], V)$. Likewise, $\{\zeta^n\}_n \subset L^2([0, 1], X)$ has a sub-sequence that converges to an element $\zeta^\infty \in L^2([0, 1], X)$. Hence, with a slight abuse of notation, we conclude that

$$\boldsymbol{\nu}^n \rightharpoonup \boldsymbol{\nu}^\infty \quad \text{and} \quad \zeta^n \rightharpoonup \zeta^\infty \quad \text{as } n \rightarrow \infty.$$

The aim is now to prove existence of minimizers by showing that $(\boldsymbol{\nu}^\infty, \zeta^\infty)$ is a minimizer to $\mathcal{J}_{\gamma, \tau}(\cdot; g): L^2([0, 1], V \times X) \rightarrow \mathbb{R}$.

Before proceeding, we introduce some notation in order to simplify the expressions. Define

$$I_t^n := I_t^{\boldsymbol{\nu}^n, \zeta^n} \quad \text{and} \quad \varphi_{s,t}^n := \varphi_{s,t}^{\boldsymbol{\nu}^n} \quad \text{for } n \in \mathbb{N} \cup \{\infty\}. \quad (9)$$

Hence, assuming geometric group action (3) and using (2), we can write

$$\mathcal{J}_{\gamma, \tau}(\boldsymbol{\nu}^n, \zeta^n; g) = \frac{\gamma}{2} \|\boldsymbol{\nu}^n\|_2^2 + \frac{\tau}{2} \|\zeta^n\|_2^2 + \mathcal{L}\left(\mathcal{A}(I_1^n \circ \varphi_{1,0}^n), g\right)$$

for $n \in \mathbb{N} \cup \{\infty\}$. Assume next that the following holds:

$$I_1^n \circ \varphi_{1,0}^n \rightharpoonup I_1^\infty \circ \varphi_{1,0}^\infty \quad \text{as } n \rightarrow \infty. \quad (10)$$

The data discrepancy term $\mathcal{L}(\cdot, g): Y \rightarrow \mathbb{R}$ is weakly lower semi continuous and the forward operator $\mathcal{A}: X \rightarrow Y$ is continuous, so $\mathcal{L}(\cdot, g) \circ \mathcal{A}$ is also weakly lower semi continuous and then (10) implies

$$\mathcal{L}(\mathcal{A}(I_1^\infty \circ \varphi_{1,0}^\infty), g) \leq \liminf_{n \rightarrow \infty} \mathcal{L}(\mathcal{A}(I_1^n \circ \varphi_{1,0}^n), g). \quad (11)$$

Furthermore, from the weak convergences of ν^n and ζ^n , we get

$$\frac{\gamma}{2} \|\nu^\infty\|_2^2 + \frac{\tau}{2} \|\zeta^\infty\|_2^2 \leq \liminf_{n \rightarrow \infty} \left[\frac{\gamma}{2} \|\nu^n\|_2^2 + \frac{\tau}{2} \|\zeta^n\|_2^2 \right]. \quad (12)$$

Hence, combining (11) and (12) we obtain

$$\mathcal{J}_{\gamma, \tau}(\nu^\infty, \zeta^\infty; g) \leq \lim_{n \rightarrow \infty} \mathcal{J}_{\gamma, \tau}(\nu^n, \zeta^n; g).$$

Since $\{(\nu^n, \zeta^n)\}_n \subset L^2([0, 1], V \times X)$ is a minimizing sequence, this yields

$$\mathcal{J}_{\gamma, \tau}(\nu^\infty, \zeta^\infty; g) = \inf_{(\nu, \zeta) \in L^2([0, 1], V \times X)} \mathcal{J}_{\gamma, \tau}(\nu, \zeta; g),$$

which proves $(\nu^\infty, \zeta^\infty) \in L^2([0, 1], V \times X)$ is a minimizer to $\mathcal{J}_{\gamma, \tau}(\cdot; g)$.

Hence, to finalize the proof we need to show that (10) holds. We start by observing that the solution of (6) can be written as

$$I_t^n := I_0^n(x) + \int_0^t \zeta^n(s, \varphi_{0,s}^n(x)) ds \quad \text{for } n \in \mathbb{N} \cup \{\infty\}, \quad (13)$$

and note that $(t, x) \mapsto I_t^n(x) \in C([0, 1] \times \Omega, \mathbb{R})$. Next, we claim that

$$I_1^n \rightharpoonup I_1^\infty \quad \text{for some } I_1^\infty \in X,$$

which is equivalent to

$$\lim_{n \rightarrow \infty} \langle I_1^n - I_1^\infty, J \rangle = 0 \quad \text{for any } J \in L^2(\Omega, \mathbb{R}). \quad (14)$$

To prove (14), note first that since continuous functions are dense in L^2 , it is enough to show (14) holds for $J \in C_0(\Omega, \mathbb{R})$. Next,

$$\langle I_1^n - I_1^\infty, J \rangle = \int_\Omega \int_0^t \left(\zeta^n(s, \varphi_{0,s}^n(x)) - \zeta^\infty(s, \varphi_{0,s}^\infty(x)) \right) J(x) ds dx \quad (15)$$

$$= \int_\Omega \int_0^t \left(\zeta^n(s, \varphi_{0,s}^n(x)) - \zeta^n(s, \varphi_{0,s}^\infty(x)) \right) J(x) ds dx \quad (16)$$

$$+ \int_\Omega \int_0^t \left(\zeta^n(s, \varphi_{0,s}^n(x)) - \zeta^\infty(s, \varphi_{0,s}^\infty(x)) \right) J(x) ds dx. \quad (17)$$

Let us now take a closer look at the term in (16):

$$\begin{aligned}
& \int_{\Omega} \int_0^t \left(\zeta^n(s, \varphi_{0,s}^n(x)) - \zeta^n(s, \varphi_{0,s}^\infty(x)) \right) J(x) ds dx \\
&= \int_{\Omega} \int_0^t \zeta^n(s, x) J(\varphi_{0,s}^n(x)) |D\varphi_{0,s}^n(x)| ds dx \\
&\quad - \int_{\Omega} \int_0^t \zeta^\infty(s, x) J(\varphi_{0,s}^\infty(x)) |D\varphi_{0,s}^\infty(x)| ds dx \\
&= \int_{\Omega} \int_0^t \zeta^n(s, x) \left(J(\varphi_{0,s}^n(x)) |D\varphi_{0,s}^n(x)| - J(\varphi_{0,s}^\infty(x)) |D\varphi_{0,s}^\infty(x)| \right) ds dx \\
&\quad - \int_{\Omega} \int_0^t \left(\zeta^\infty(s, x) - \zeta^n(s, x) \right) J(\varphi_{0,s}^\infty(x)) |D\varphi_{0,s}^\infty(x)| ds dx \\
&= \langle \zeta^n, J^n - J^\infty \rangle - \langle \zeta^\infty - \zeta^n, J^\infty \rangle
\end{aligned}$$

where $J^n \in L^2([0, 1], X)$ is defined as

$$J^n(s, x) := J(\varphi_{s,0}^n(x)) |D\varphi_{s,0}^n(x)| \quad \text{for } n \in \mathbb{N} \setminus \{\infty\}. \quad (18)$$

By proposition 3 we know that $\varphi_{s,0}^n \rightarrow \varphi_{s,0}^\infty$ and $D\varphi_{s,0}^n \rightarrow D\varphi_{s,0}^\infty$ uniformly on Ω . Since J is continuous on Ω , we conclude that $\|J^n - J^\infty\|_2$ tends to 0. Since ζ^n is bounded, we conclude that

$$\langle \zeta^n, J^n - J^\infty \rangle \leq \|\zeta^n\|_2 \cdot \|J^n - J^\infty\|_2 \rightarrow 0.$$

Furthermore, since $\zeta^n \rightarrow \zeta^\infty$, we also get $\langle \zeta^\infty - \zeta^n, J^\infty \rangle \rightarrow 0$. Hence, we have shown that (16) tends to zero, i.e.,

$$\lim_{n \rightarrow \infty} \int_{\Omega} \int_0^t \left(\zeta^n(s, \varphi_{0,s}^n(x)) - \zeta^n(s, \varphi_{0,s}^\infty(x)) \right) J(x) ds dx = 0.$$

Finally, we consider the term in (17). Since $\zeta^n \rightarrow \zeta^\infty$, we immediately obtain

$$\int_{\Omega} \int_0^t \left(\zeta^n(s, \varphi_s^\infty(x)) - \zeta^\infty(s, \varphi_s^\infty(x)) \right) J(x) ds dx = \langle \zeta^n - \zeta^\infty, J^\infty \rangle \rightarrow 0.$$

To summarise, we have just proved that both terms (16) and (17) tend to 0 as $n \rightarrow \infty$, which implies that (14) holds, i.e., $I_1^n \rightarrow I_1^\infty$.

To prove (10), i.e., $I_1^n \circ \varphi_{1,0}^n \rightarrow I_1^\infty \circ \varphi_{1,0}^\infty$, we need to show that

$$\lim_{n \rightarrow \infty} \langle I_1^n \circ \varphi_{1,0}^n - I_1^\infty \circ \varphi_{1,0}^\infty, J \rangle = 0 \quad \text{for any } J \in L^2(\Omega, \mathbb{R}), \quad (19)$$

and as before, we may assume $J \in C_0(\Omega, \mathbb{R})$. Using (18) we can express the term in (19) whose limit we seek as

$$\begin{aligned}
& \left| \langle I_1^n \circ \varphi_{1,0}^n - I_1^\infty \circ \varphi_{1,0}^\infty, J \rangle \right| \\
& \leq \left| \langle I_1^n, J^n(1, \cdot) - J^\infty(1, \cdot) \rangle \right| + \left| \langle I_1^n - I_1^\infty, J^\infty(1, \cdot) \rangle \right| \\
& \leq \|I_1^n\| \cdot \|J^n(1, \cdot) - J^\infty(1, \cdot)\| + |\langle I_1^n - I_1^\infty, J^\infty(1, \cdot) \rangle|.
\end{aligned}$$

Since $\|I_1^n\|$ is bounded (because $\|\zeta^n\|$ is bounded) and since $I_1^n \rightarrow I_1^\infty$ (which we shoed before), all terms above tend to 0 as $n \rightarrow \infty$, i.e., (19) holds.

This concludes the proof of (10), which in turn implies the existence of a minimizer of $\mathcal{J}_{\gamma,\tau}(\cdot; g)$. \square

Our next result shows that the solution to the indirect registration problem is (weakly) continuous w.r.t. variations in data, and as such, it is a kind of stability result.

Proposition 5 (Stability). *Let $\{g_k\}_k \subset Y$ and assume this sequence converges (in norm) to some $g \in Y$. Next, for each $\gamma, \tau > 0$ and each k , define $(\nu^k, \zeta^k) \in L^2([0, 1], V \times X)$ as*

$$(\nu^k, \zeta^k) = \arg \min_{(\nu, \zeta)} \mathcal{J}_{\gamma,\tau}(\nu, \zeta; g_k).$$

Then there exists a sub sequence of (ν^k, ζ^k) that converges weakly to a minimizer of $\mathcal{J}_{\gamma,\tau}(\cdot; g)$ in (7).

Proof. $\mathcal{J}_{\gamma,\tau}(\cdot; g_k)$ has a minimizer $(\nu^k, \zeta^k) \in L^2([0, 1], V \times X)$ for any $g_k \in Y$ (proposition 4). The idea is first to show that the sequences $(\nu^k)_k$ and $(\zeta^k)_k$ are bounded. Next, we show that there exists a weakly converging subsequence of (ν^k, ζ^k) that converges to a minimizer (ν, ζ) of $\mathcal{J}_{\gamma,\tau}(\cdot; g)$, which also exists due to proposition 4.

Since (ν^k, ζ^k) minimizes $\mathcal{J}_{\gamma,\tau}(\cdot; g_k)$, by (7) we have

$$\|\nu^k\|_2^2 \leq \frac{2}{\gamma} \mathcal{J}_{\gamma,\tau}(\cdot; g_k)(\nu^k, \zeta^k) \leq \frac{2}{\gamma} \mathcal{J}_{\gamma,\tau}(\cdot; g_k)(\mathbf{0}, 0) \quad \text{for each } k. \quad (20)$$

Observe now that if $\nu = \mathbf{0}$ and $\zeta = 0$, then $\varphi_{0,1}^\nu = \text{Id}$ by (1) and $I_1^{\nu,\zeta} = I_0$ by (6), so in particular

$$\mathcal{W}(\varphi_{0,1}^\nu, I_1^{\nu,\zeta}) = I_0 \quad \text{whenever } \nu = \mathbf{0} \text{ and } \zeta = 0,$$

Hence, $\mathcal{J}_{\gamma,\tau}(\cdot; g_k)(\mathbf{0}, 0) = \mathcal{L}(\mathcal{A}(I_0), g_k)$ and, in addition, $\|\nu\|_2 = 0$ and $\|\zeta\|_2 = 0$, so (20) becomes

$$\|\nu^k\|_2^2 \leq \frac{2}{\gamma} \mathcal{L}(\mathcal{A}(I_0), g_k) \rightarrow \mathcal{L}(\mathcal{A}(I_0), g) \quad \text{as } k \rightarrow \infty. \quad (21)$$

In conclusion, the sequence $(\nu^k)_k \subset L^2([0, 1], V)$ is bounded. In a similar way, we can show that $(\zeta^k)_k \subset L^2([0, 1], X)$ is bounded.

The boundedness of both sequences implies that there are sub sequences to these that converge weakly to some element $\nu^\infty \in L^2([0, 1], V)$ and $\zeta^\infty \in L^2([0, 1], X)$, respectively. Thus, to complete the proof, we need to show that $(\nu^\infty, \zeta^\infty) \in L^2([0, 1], V \times X)$ minimizes $\mathcal{J}_{\gamma,\tau}(\cdot; g)$, i.e., that

$$\mathcal{J}_{\gamma,\tau}(\nu^\infty, \zeta^\infty; g) \leq \mathcal{J}_{\gamma,\tau}(\nu, \zeta; g) \quad \text{holds for any } (\nu, \zeta) \in L^2([0, 1], V \times X).$$

From the weak convergences, we obtain

$$\begin{aligned} \frac{\gamma}{2} \|\boldsymbol{\nu}^\infty\|_2^2 + \frac{\tau}{2} \|\zeta^\infty\|_2^2 &\leq \frac{\gamma}{2} \liminf_k \|\boldsymbol{\nu}^k\|_2^2 + \frac{\tau}{2} \liminf_k \|\zeta^k\|_2^2 \\ &\leq \frac{1}{2} \liminf_k \left[\gamma \|\boldsymbol{\nu}^k\|_2^2 + \tau \|\zeta^k\|_2^2 \right]. \end{aligned} \quad (22)$$

The weak convergence also implies (see proof of proposition 4) that

$$\mathcal{W}(\varphi_{0,1}^k, I_1^\infty) \rightharpoonup \mathcal{W}(\varphi_{0,1}^\infty, I_1^\infty) \quad \text{in } X.$$

In the above, we have used the notational convention introduced in (9). By the lower semi-continuity of \mathcal{L} , we get

$$\mathcal{L}\left(\mathcal{A}(\mathcal{W}(\varphi_{0,1}^\infty, I_1^\infty)), g\right) \leq \liminf_k \mathcal{L}\left(\mathcal{A}(\mathcal{W}(\varphi_{0,1}^k, I_1^k)), g_k\right). \quad (23)$$

Hence,

$$\begin{aligned} \mathcal{J}_{\gamma,\tau}(\boldsymbol{\nu}^\infty, \zeta^\infty; g) &= \frac{\gamma}{2} \|\boldsymbol{\nu}^\infty\|_2^2 + \frac{\tau}{2} \|\zeta^\infty\|_2^2 + \mathcal{L}\left(\mathcal{A}(\mathcal{W}(\varphi_{0,1}^\infty, I_1^\infty)), g\right) \\ &\leq \frac{1}{2} \liminf_k \left[\gamma \|\boldsymbol{\nu}^k\|_2^2 + \tau \|\zeta^k\|_2^2 \right] + \liminf_k \mathcal{L}\left(\mathcal{A}(\mathcal{W}(\varphi_{0,1}^k, I_1^k)), g_k\right) \\ &\leq \liminf_k \mathcal{J}_{\gamma,\tau}(\boldsymbol{\nu}^k, \zeta^k; g_k). \end{aligned} \quad (24)$$

Next, since $(\boldsymbol{\nu}^k, \zeta^k) \in L^2([0, 1], V \times X)$ minimizes $\mathcal{J}_{\gamma,\tau}(\cdot; g_k)$, we get

$$\mathcal{J}_{\gamma,\tau}(\boldsymbol{\nu}^\infty, \zeta^\infty; g) \leq \liminf_k \mathcal{J}_{\gamma,\tau}(\boldsymbol{\nu}, \zeta; g_k)$$

for any $(\boldsymbol{\nu}, \zeta) \in L^2([0, 1], V \times X)$. Furthermore,

$$\mathcal{J}_{\gamma,\tau}(\boldsymbol{\nu}, \zeta; g_k) \rightarrow \mathcal{J}_{\gamma,\tau}(\boldsymbol{\nu}, \zeta; g),$$

so

$$\mathcal{J}_{\gamma,\tau}(\boldsymbol{\nu}^\infty, \zeta^\infty; g) \leq \mathcal{J}_{\gamma,\tau}(\boldsymbol{\nu}, \zeta; g) \quad \text{for all } (\boldsymbol{\nu}, \zeta) \in L^2([0, 1], V \times X).$$

In particular, we have shown that $(\boldsymbol{\nu}^\infty, \zeta^\infty)$ minimises $\mathcal{J}_{\gamma,\tau}(\cdot; g)$. \square

Our final results concerns convergence, which investigates the behaviour of the solution as data error tends to zero and regularization parameters are adapted accordingly through a parameter choice rule against the data error.

Proposition 6 (Convergence). *Let $g \in Y$ and assume*

$$\mathcal{A}(\mathcal{W}(\varphi_{0,1}^{\boldsymbol{\nu}, \zeta}, I_1^{\boldsymbol{\nu}, \zeta})) = g \quad \text{for some } (\boldsymbol{\nu}, \zeta) \in L^2([0, 1], V \times X).$$

Next, for parameter choice rules $\delta \mapsto \gamma(\delta)$ and $\delta \mapsto \tau(\delta)$ with $\delta > 0$, define

$$(\boldsymbol{\nu}_\delta, \zeta_\delta) \in \arg \min_{(\boldsymbol{\nu}, \zeta)} \mathcal{J}_{\gamma(\delta), \tau(\delta)}(\boldsymbol{\nu}, \zeta; g + e_\delta)$$

where $e_\delta \in Y$ (data error) has magnitude $\|e_\delta\| = \delta$. Finally, assume that $\delta \mapsto \gamma(\delta)/\tau(\delta)$ and $\delta \mapsto \tau(\delta)/\gamma(\delta)$ are bounded, and

$$\lim_{\delta \rightarrow 0} \gamma(\delta) = \lim_{\delta \rightarrow 0} \tau(\delta) = \lim_{\delta \rightarrow 0} \frac{\delta^2}{\gamma(\delta)} = \lim_{\delta \rightarrow 0} \frac{\delta^2}{\tau(\delta)} = 0.$$

Then, for any sequence $\delta_k \rightarrow 0$ there exists a sub-sequence $\delta_{k'}$ such that $(\boldsymbol{\nu}_{\delta_{k'}}, \zeta_{\delta_{k'}})$ converges weakly to a $(\boldsymbol{\nu}^*, \zeta^*)$ satisfying $\mathcal{A}(\mathcal{W}(\varphi_{0,1}^{\boldsymbol{\nu}^*}, I_1^{\boldsymbol{\nu}^*, \zeta^*})) = g$.

Proof. Let (δ_k) be a sequence converging to 0 and, for each k , let us denote

$$g_k := g + e_{\delta_k}, \quad \boldsymbol{\nu}^k := \boldsymbol{\nu}_{\delta_k}, \quad \text{and} \quad \zeta^k := \zeta_{\delta_k}.$$

Similarly to previous proofs, we will show that the sequences $(\boldsymbol{\nu}^k)$ and (ζ^k) are bounded, and then that the weakly converging subsequence that can be extracted from $(\boldsymbol{\nu}^k, \zeta^k)$ converges to a suitable solution.

Define $\gamma_k := \gamma(\delta_k)$ and $\tau_k := \tau(\delta_k)$. Then, for each k we have

$$\begin{aligned} \|\boldsymbol{\nu}^k\|_2^2 &\leq \frac{1}{\gamma_k} \mathcal{J}_{\gamma_k, \tau_k, g_k}(\boldsymbol{\nu}^k, \zeta^k) \leq \frac{1}{\gamma_k} \mathcal{J}_{\gamma_k, \tau_k, g_k}(\widehat{\boldsymbol{\nu}}, \widehat{\zeta}) \\ &= \frac{1}{\gamma_k} \left(\gamma_k \|\widehat{\boldsymbol{\nu}}\|_2^2 + \tau_k \|\widehat{\zeta}\|_2^2 + \mathcal{L}(g, g_k) \right) \leq \|\widehat{\boldsymbol{\nu}}\|_2^2 + \frac{\tau_k}{\gamma_k} \|\widehat{\zeta}\|_2^2 + \frac{\delta_k}{\gamma_k}. \end{aligned}$$

From the assumptions on the parameter choice rules, we conclude that $(\boldsymbol{\nu}^k) \subset L^2([0, 1], V)$ is bounded. Similarly, one can show that $(\zeta^k) \subset L^2([0, 1], X)$ is bounded.

From the above, we conclude that there is a subsequence of $(\boldsymbol{\nu}^k, \zeta^k)$ that converges weakly to $(\widetilde{\boldsymbol{\nu}}, \widetilde{\zeta})$ in $L^2([0, 1], V) \times L^2([0, 1], V)$. Then (see proof of proposition 4)

$$\mathcal{L}\left(\mathcal{A}(\mathcal{W}(\varphi_{0,1}^{\widetilde{\boldsymbol{\nu}}}, I_1^{\widetilde{\boldsymbol{\nu}}, \widetilde{\zeta}})), g\right) \leq \liminf_k \mathcal{L}\left(\mathcal{A}(\mathcal{W}(\varphi_{0,1}^{\boldsymbol{\nu}^k}, I_1^{\boldsymbol{\nu}^k, \zeta^k})), g_k\right).$$

Furthermore, the above quantity converges to 0 since

$$\begin{aligned} \mathcal{L}\left(\mathcal{A}(\mathcal{W}(\varphi_{0,1}^{\boldsymbol{\nu}^k}, I_1^{\boldsymbol{\nu}^k, \zeta^k})), g_k\right) &\leq \mathcal{J}_{\gamma_k, \tau_k, g_k}(\boldsymbol{\nu}^k, \zeta^k) \leq \mathcal{J}_{\gamma_k, \tau_k, g_k}(\widehat{\boldsymbol{\nu}}, \widehat{\zeta}) \\ &= \gamma_k \|\widehat{\boldsymbol{\nu}}\|_2^2 + \tau_k \|\widehat{\zeta}\|_2^2 + \mathcal{L}(g, g_k) \rightarrow 0 \quad \text{and} \quad k \rightarrow \infty. \end{aligned}$$

Hence, $\mathcal{A}(\mathcal{W}(\varphi_{0,1}^{\widetilde{\boldsymbol{\nu}}}, I_1^{\widetilde{\boldsymbol{\nu}}, \widetilde{\zeta}})) = g$. \square

4.4 Numerical implementation

In order to solve (8), we use a gradient descent scheme on the variable $(\boldsymbol{\nu}, \zeta) \in L^2([0, 1], V \times X)$ with a uniform discretization of the interval $[0, 1]$ into N parts, i.e., $t_i = 1/N$ for $i = 0, \dots, N$ and the gradient descent is performed on $\boldsymbol{\nu}(t_i, \cdot)$, $\zeta(t_i, \cdot)$, for $i = 0, 1, \dots, N$. An alternative approach

developed in [18] extends the time discrete path method in [11] to the indirect setting.

In order to compute numerical integrations, we use a Euler scheme on this discretization. The flow equation (1) is computed using the following approximation with small deformations: $\varphi_{t_i,0}^{\nu} \approx \varphi_{t_{i-1},0}^{\nu} \circ \left(\text{Id} - \frac{1}{N} \nu(t_{i-1}, \cdot) \right)$.

Algorithm 1 presents the implementation¹ for computing the gradient of \mathcal{J} and it is based on expressions from appendix A). The computation of the Jacobian determinant $|\text{Det}(d\varphi_{t_i,1}^{\nu}(x))|$ at each time point is based on the following approximation similar to [9]:

$$|\text{Det}(d\varphi_{t_i,1}^{\nu}(x))| \approx \left(1 + \frac{1}{N} \text{div} \nu(t_i, \cdot) \right) |D\varphi_{t_{i+1},1}^{\nu}| \circ \left(\text{Id} + \frac{1}{N} \nu(t_i, \cdot) \right).$$

5 Application to 2D tomography

5.1 The setting

The forward operator Let $X = L^2(\Omega, \mathbb{R})$ whose elements represent 2D images on a fixed bounded domain $\Omega \subset \mathbb{R}^2$. In the application shown here, diffeomorphisms act on X through a geometric group action in (3) and the goal is to register a given differentiable template image $I_0 \in X$ against a target that observed indirectly as in (4).

The forward operator $\mathcal{A}: X \rightarrow Y$ in 2D tomographic imaging is the 2D ray/Radon transform, i.e.,

$$\mathcal{A}(f)(\omega, x) = \int_{\mathbb{R}} f(x + s\omega) ds \quad \text{for } \omega \in S^1 \text{ and } x \in \omega^{\perp}.$$

Here, S^1 is the unit circle, so (ω, x) encodes the line $s \mapsto x + s\omega$ in \mathbb{R}^2 with direction ω through x . The data manifold M is the set of such lines that are included in the measurements, i.e., M is given by the experimental set-up. We will consider parallel lines in \mathbb{R}^2 (parallel beam data), i.e., tomographic data are noisy digitized values of an L^2 -function on this manifold so $g \in Y = L^2(M, \mathbb{R})$. The forward operator is linear, so it is particular Gateaux differentiable, and the adjoint of its derivative is given by the backprojection, see [17, 15] for further details.

If data is corrupted by additive Gaussian noise, so a suitable data likelihood is the 2-norm, i.e.,

$$\mathcal{L}: Y \times Y \rightarrow \mathbb{R} \quad \text{with} \quad \mathcal{L}(g, h) = \|g - h\|_2^2.$$

The noise level in data is specified by the peak signal-to-noise ratio (PSNR), which is defined as

$$\text{PSNR}(g) = 10 \log_{10} \left(\frac{\|g_0 - \bar{g}_0\|^2}{\|e - \bar{e}\|^2} \right) \quad \text{for } g = g_0 + e.$$

¹<https://github.com/bgris/odl/tree/IndirectMatching/examples/Metamorphosis>

Algorithm 1 Computation of $\nabla \mathcal{J}(\boldsymbol{\nu}, \zeta)$.

Require: $\boldsymbol{\nu}(t_i, \cdot)$ and $\zeta(t_i, \cdot)$ with $t_i \leftarrow i/N$ for $i = 0, 1, \dots, N$.

```

1: for  $i = 1, \dots, N$  do ▷ Compute  $\zeta(t_i, \cdot) \circ \varphi_{0, t_i}^\nu$ 
2:    $temp \leftarrow \zeta(t_i, \cdot)$ 
3:   for  $j = i - 1, \dots, 0$  do
4:      $temp \leftarrow temp \circ \left( \text{Id} + \frac{1}{N} \boldsymbol{\nu}(t_j, \cdot) \right)$ 
5:   end for
6:    $\zeta(t_i, \cdot) \circ \varphi_{0, t_i}^\nu \leftarrow temp$ 
7: end for
8: for  $i = 1, \dots, N$  do ▷ Compute  $f^{\boldsymbol{\nu}, \zeta}(t_i, \cdot) := I^{\boldsymbol{\nu}, \zeta}(t_i, \cdot) \circ \varphi_{0, t_i}^\nu$ 
9:    $I^{\boldsymbol{\nu}, \zeta}(t_i, \cdot) \leftarrow I_0 + \sum_{j=0}^{i-1} I^{\boldsymbol{\nu}, \zeta}(t_j, \cdot) + \frac{1}{N} \zeta(t_j, \cdot) \circ \varphi_{0, t_j}^\nu$ 
10:   $I^{\boldsymbol{\nu}, \zeta}(t_i, \cdot) \circ \varphi_{0, 0}^\nu \leftarrow I^{\boldsymbol{\nu}, \zeta}(t_i, \cdot)$ 
11:  for  $j = 1, \dots, i$  do
12:     $I^{\boldsymbol{\nu}, \zeta}(t_i, \cdot) \circ \varphi_{t_j, 0}^\nu \leftarrow \left( I^{\boldsymbol{\nu}, \zeta}(t_i, \cdot) \circ \varphi_{0, t_{j-1}}^\nu \right) \circ \left( \text{Id} - \frac{1}{N} \boldsymbol{\nu}(t_{j-1}, \cdot) \right)$ 
13:  end for
14: end for
15: for  $i = 1, \dots, N$  do ▷ Compute  $I_0 \circ \varphi_{t_i, 0}^\nu$ 
16:    $I_0 \circ \varphi_{0, 0}^\nu \leftarrow I_0 \circ \varphi_{0, 0}^\nu = I_0$ 
17:    $I_0 \circ \varphi_{t_i, 0}^\nu \leftarrow \left( I_0 \circ \varphi_{t_{i-1}, 0}^\nu \right) \circ \left( \text{Id} - \frac{1}{N} \boldsymbol{\nu}(t_{i-1}, \cdot) \right)$ 
18: end for
19: for  $i = 1, \dots, N$  do
20:    $G(t_i, \cdot) \leftarrow \nabla(I_0 \circ \varphi_{t_i, 0}^\nu) + \sum_{j=0}^{i-1} \frac{1}{N} \nabla(\zeta(t_j, \cdot) \circ \varphi_{t_i, t_j}^\nu)$ 
21: end for
22:  $|\text{D}\varphi_{t_N, 1}^\nu| = |\text{D}\varphi_{1, 1}^\nu| = 1$  ▷ Compute  $|\text{D}\varphi_{t_i, 1}^\nu|$ 
23: for  $i = N - 1, \dots, 0$  do
24:    $|\text{D}\varphi_{t_i, 1}^\nu| \leftarrow \left( 1 + \frac{1}{N} \text{div} \boldsymbol{\nu}(t_i, \cdot) \right) |\text{D}\varphi_{t_{i+1}, 1}^\nu| \circ \left( \text{Id} + \frac{1}{N} \boldsymbol{\nu}(t_i, \cdot) \right)$ 
25: end for
26:  $\nabla \mathcal{L}(f^{\boldsymbol{\nu}, \zeta}(1, \cdot), g)(\varphi_{t_N, 1}^\nu) \leftarrow \nabla \mathcal{L}(f^{\boldsymbol{\nu}, \zeta}(1, \cdot), g)$ 
27: for  $i = N - 1, \dots, 0$  do ▷ Compute  $\nabla \mathcal{L}(f^{\boldsymbol{\nu}, \zeta}(1, \cdot), g)(\varphi_{t_i, 1}^\nu)$ 
28:    $\nabla \mathcal{L}(f^{\boldsymbol{\nu}, \zeta}(1, \cdot), g)(\varphi_{t_i, 1}^\nu) \leftarrow \nabla \mathcal{L}(f^{\boldsymbol{\nu}, \zeta}(1, \cdot), g)(\varphi_{t_{i+1}, 1}^\nu) \circ \left( \text{Id} + \frac{1}{N} \boldsymbol{\nu}(t_i, \cdot) \right)$ 
29: end for
30: for  $i = 1, \dots, N$  do ▷ Compute  $\nabla \mathcal{J}(\boldsymbol{\nu}, \zeta)$ 
31:

```

$$\begin{aligned} \nabla_{\boldsymbol{\nu}} \mathcal{J}_{\gamma, \tau}(\boldsymbol{\nu}, \zeta, g)(t_i, \cdot) &\leftarrow 2\gamma \boldsymbol{\nu}(t_i, \cdot) \\ &\quad - \int_{\Omega} K(x, \cdot) \left| \text{Det}(\text{d}\varphi_{t_i, 1}^\nu(x)) \right| \nabla \mathcal{L}(f^{\boldsymbol{\nu}, \zeta}(1, \cdot), g)(\varphi_{t_i, 1}^\nu(x)) G(t_i, x) dx \end{aligned}$$

32:

$$\begin{aligned} \nabla_{\zeta} \mathcal{J}_{\gamma, \tau}(\boldsymbol{\nu}, \zeta)(t_i, \cdot) &\leftarrow 2\tau \zeta(t_i, \cdot) \\ &\quad + \left| \text{Det}(\text{d}\varphi_{t_i, 1}^\nu) \right| \nabla \mathcal{L}(f^{\boldsymbol{\nu}, \zeta}(1, \cdot), g)(\varphi_{t_i, 1}^\nu(x)) G(t_i, \cdot) \end{aligned}$$

33: **end for**

34: **return** $\nabla \mathcal{J}(\boldsymbol{\nu})(t_i, \cdot), \nabla \mathcal{J}(\zeta)(t_i, \cdot)$ for $i = 1, \dots, N$.

In the above, g_0 is the noise-free part and e is the noise component of data with $\overline{g_0}$ and \overline{e} denoting the mean of g_0 and e , respectively. The PSNR is expressed in terms of dB.

Joint tomographic reconstruction and registration Under the geometric group action (3), metamorphosis based-indirect registration reads as

$$f_1^{\widehat{\nu}, \widehat{\zeta}} = \mathcal{W}(\varphi_{0,1}^{\widehat{\nu}}, I_1^{\widehat{\nu}, \widehat{\zeta}}) = I_1^{\widehat{\nu}, \widehat{\zeta}} \circ \varphi_{1,0}^{\widehat{\nu}}$$

where $(\widehat{\nu}, \widehat{\zeta}) \in L^2([0, 1], V \times X)$ minimizes (7), i.e., given regularization parameters $\gamma, \tau \geq 0$ and initial template $I_0 \in X$ we solve

$$\min_{(\nu, \zeta)} \left[\frac{\gamma}{2} \|\nu\|_2^2 + \frac{\tau}{2} \|\zeta\|_2^2 + \left\| \mathcal{A} \left(f(1, \phi(1, \cdot)^{-1}) \right) - g \right\|_2^2 \right]$$

$$\begin{cases} \frac{d}{dt} f(t, x) = \zeta(t, \phi(t, x)) \\ f(0, x) = I_0(x) \\ \frac{d}{dt} \phi(t, x) = \nu(t, \phi(t, x)) \\ \phi(0, x) = x. \end{cases} \quad (25)$$

We will consider a set V of vector fields that is an RKHS with a reproducing kernel represented by symmetric and positive definite Gaussian. Then V is admissible and is continuously embedded in $L^2(\Omega, \mathbb{R}^2)$. The kernel we pick is $K_\sigma: \Omega \times \Omega \rightarrow \mathbb{R}_+^{2 \times 2}$

$$K_\sigma(x, y) := \exp\left(-\frac{1}{2\sigma^2} \|x - y\|_2\right) \begin{pmatrix} 1 & 0 \\ 0 & 1 \end{pmatrix} \quad \text{for } x, y \in \mathbb{R}^2 \text{ and } \sigma > 0. \quad (26)$$

The kernel-size σ also acts as a regularization parameter.

5.2 Overview of experiments

In the following we perform a number of experiments that tests various aspects of using metamorphoses based indirect registration for joint tomographic reconstruction and registration. The tomographic inverse problem along with characteristics of the data are outlined in section 5.1. The results are obtained by solving (25) via a gradient descent, see appendix A for the computation of the gradient of the objective. For each reconstruction, we list the the number of angles of the parallel beam ray transform, the kernel-size σ in (26), and the two regularisation parameters $\gamma, \tau > 0$ appearing in the objective functional in (25).

The first test (section 5.3) aims to show how metamorphoses based indirect registration handles a template that has intensities differing from those of the target. Section 5.4 considers the ability to handle an initial template with a topology that does not match the target. This is essential when one has simultaneous geometric and topological changes. As an example, in spatiotemporal imaging it may very well be the case that geometric deformation takes place simultaneously as new masses appear or disappear. Next, in section 5.5 studies the robustness of the solutions with respect to variations in the regularization parameters. Finally, section 5.6 shows how indirect registration through metamorphoses can be used to recover a temporal evolution of a given template registered against time series of data. This is an essential part of spatio-temporal tomographic reconstruction.

Sections 5.3 to 5.5 have a common setting in that grey scale images in the reconstruction space are discretised using 256×256 pixels in the image domain $\Omega = [-16, 16] \times [-16, 16]$. The tomographic data is noisy samples of the 2D parallel beam ray transform of the target sampled at 100 angles uniformly distributed angles in $[0, \pi]$ with 362 lines/angle. Data is corrupted with additive Gaussian noise with differing noise levels.

5.3 Consistent topology and inconsistent intensities

Here, topology of the template is consistent with that of the target, but intensities differ. The template, which is shown in fig. 2(a), is registered against tomographic data shown in fig. 2(c). The (unknown) target used to generate data is shown in fig. 2(b). Also, data has a noise level corresponding to a PSNR of 15.6 dB and kernel size is $\sigma = 2$, which should be compared to the size of the image domain $\Omega = [-16, 16] \times [-16, 16]$. The final reconstruction is shown in fig. 2(h), which is to be compared against the target in fig. 2(b). Figure 2 also shows image, deformation and template trajectories.

We clearly see that metamorphosis based indirect registration can handle a template with wrong intensities. As a comparison, see fig. 1(c) for the corresponding LDDMM based indirect registration using the same template and data. Furthermore, the different trajectories also provides easy visual interpretation of the influence of geometric and intensity deformations.

5.4 Inconsistent topology and intensities

Here, both topology and intensities of the template differ from those in the target. The template, which is shown in fig. 3(a), is registered against tomographic data shown in fig. 3(c). The (unknown) target used for generating the data is shown in fig. 3(b). Also, data has a noise level corresponding to a PSNR of 10.6 dB and kernel size is $\sigma = 2$, which should be compared to the size of the image domain $\Omega = [-16, 16] \times [-16, 16]$. The final reconstruction

$\tau \backslash \gamma$	10^{-7}	10^{-5}	10^{-3}	10^{-1}
10^{-1}	0.767 -6.37	0.768 -6.43	0.768 -6.422	0.768 -6.42
10^{-3}	0.766 -6.33	0.770 -6.36	0.770 -6.36	0.770 -6.36
10^{-5}	0.766 -6.33	0.770 -6.35	0.770 -6.36	0.770 -6.36
10^{-7}	0.766 -6.33	0.770 -6.35	0.770 -6.36	0.770 -6.36

Table 1: SSIM (top) and PSNR (bottom) values for metamorphosis based indirect registration with varying regularisation parameter and $\sigma = 3$ for several regularisation parameters.

is shown in fig. 3(h), which is to be compared against the target in fig. 3(b). Figure 3 also shows image, deformation and template trajectories.

We clearly see that metamorphosis based indirect registration can handle a template where both intensities and the topology are wrong. In particular, we can see follow both the deformation of the template and the appearance of the white disc.

5.5 Robustness

Metamorphosis based indirect registration, which amounts to solving (25), requires selecting three parameters: the kernel-size σ and the two regularisation parameters γ and τ . Here we study the influence of these parameters on the final registered image (reconstruction) based on the setup in section 5.4.

The reconstruction along with its template and deformation parts are not that sensitive to the specific choice the two regularisation parameters γ and τ , see table 1 that shows the structural similarity (SSIM) and PSNR values for various values of γ and τ when $\sigma = 3$. The reconstruction is on the other hand more sensitive to the choice of the kernel size, see table 2 for a table of SSIM and PSNR values corresponding to different choices of kernel size. Figure 4 also shows reconstructed image with the corresponding final template and deformation parts for various values of σ . Interestingly, even if the reconstruction is satisfying for the various values of the kernel size σ , its template part and deformation parts are really different. The geometric deformation and the change in intensity values seem to balance in a non-intuitive way in order to produce a reasonable final image.

σ	0.3	0.6	1	2	3	5	10
SSIM	0.660	0.703	0.737	0.769	0.766	0.764	0.682
PSNR	-7.75	-7.03	-6.57	-6.36	-6.49	-6.66	-8.98

Table 2: SSIM and PSNR values for metamorphosis based indirect registration with varying kernel size σ and fixed regularisation parameters $\gamma = \tau = 10^{-5}$.

5.6 Spatio-temporal reconstruction

The goal here is to recover the unknown temporal evolution of a template matched against (gated) parallel beam 2D ray transform data acquired at 10 different time points (from $t = 0.1$ to $t = 1$), so the target undergoes a temporal evolution. At each of the 10 time points, we only have limited tomographic data in the sense that i :th acquisition corresponds to sampling the parallel beam ray transform of the target at time t_i using 10 angles randomly distributed in $[(i-1)\pi/10, i\pi/10]$ using 362 lines/angles. Similarly to previous experiments, the reconstruction space is $\Omega = [-16, 16] \times [-16, 16]$, discretised as 256×256 pixel grey scale images.

The registration of the template I_0 against the temporal series of data g_i , $1 \leq i \leq 10$ at the 10 time points t_i is performed by minimizing the following functional with respect to *one* trajectory $(\nu, \zeta) \in L^2([0, 1], V \times X)$:

$$\mathcal{J}_{\gamma, \tau}(\nu, \zeta; g_1, \dots, g_{10}) := \frac{\gamma}{2} \|\nu\|_2^2 + \frac{\tau}{2} \|\zeta\|_2^2 + \sum_{i=1}^{10} \mathcal{L}\left(\mathcal{A}(\mathcal{W}(\varphi_{0,t_i}^\nu, I_{t_i}^{\nu, \zeta})), g_i\right)$$

where $t \mapsto I_t^{\nu, \zeta}$, is the absolutely continuous solution to

$$\begin{cases} \frac{d}{dt} I_t^{\nu, \zeta}(x) = \zeta(t, \varphi_{0,t}^\nu(x)) \\ I_0^{\nu, \zeta}(x) = I_0(x) \end{cases} \quad \text{with } \varphi_{0,t}^\nu \in G_V \text{ as in (2).}$$

The target, the gated tomographic data, and the three trajectories (image, deformation and template) resulting from the metamorphosis based indirect registration are shown in fig. 5. We see that metamorphosis based indirect registration can be used for spatio-temporal reconstruction even when (gated) data is highly under sampled. In particular, we can recover the evolution (both the geometric deformation and the appearance of the white disc) of the target. As a comparison, fig. 5(f) presents reconstructions obtained from filtered back projection (FBP) and total variation (TV). Here, data is a concatenation of the 10 gated data sets, thereby corresponding then sampling the ray transform using 100 angles in $[0, \pi]$. Note however that the temporal evolution of the target is not accounted for in these reconstructions.

6 Conclusions and discussion

We introduced a metamorphosis-based framework for indirect registration and showed that this corresponds to a well-defined regularization method. We also present several numerical examples from tomography.

In particular, section 5.6 illustrates that this framework enables to recover the temporal evolution of a template from temporal data, even when data are very limited for each time point. This approach assumes that one has access to an initial template. In spatio-temporal reconstruction, such an initial template is unknown and it needs to be recovered as well. One approach for doing this is by an intertwined scheme that alternates between to steps (similarly to [14]): (i) given a template, estimate its evolution that is consistent with times series of data using the metamorphosis framework for indirect registration, and (ii) estimate the initial template from times series of data given its evolution. The approach in section 5.6 solves the first step, which is the more difficult one.

Another topic is the choice of hyperparameters. Our metamorphosis-based framework for indirect registration relies on three parameters, but as shown in section 5.5, the most important one is the kernel-size σ . The latter has a strong influence on the way the reconstructed image trajectory decomposes into a deformation and a template part. Clearly it acts as a regularisation parameter and a natural problem is to devise a scheme for choosing it depending on the size of features (scale) undergoing deformation. Unfortunately, similarly to direct registration using the LDDMM framework, the choice of this parameter (and more generally choice of kernel for the RKHS V) is still an open problem [3, 9, 10]. One way is to use a multi-scale approach [7, 20, 22] but a general method for selecting an appropriate kernel-size remains to be determined.

7 Acknowledgements

The work by Ozan Öktem, Barbara Gris and Chong Chen was supported by the Swedish Foundation for Strategic Research grant AM13-0049.

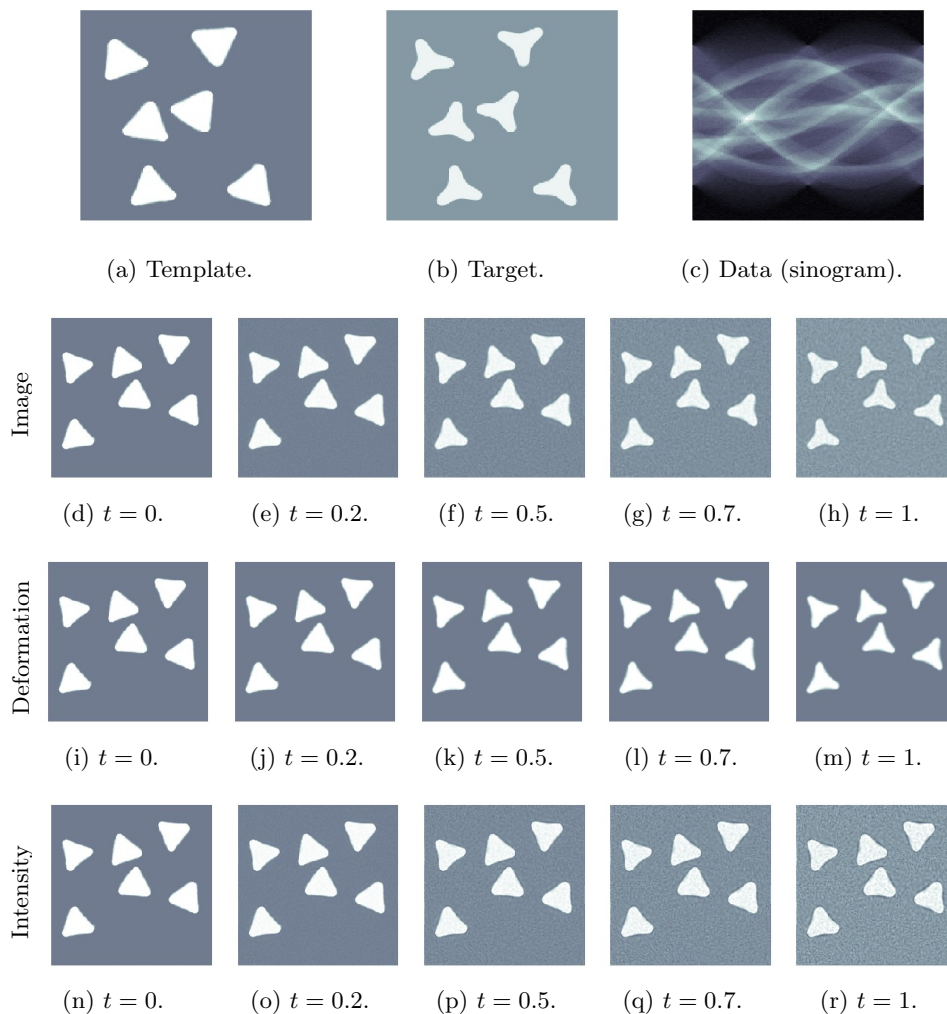


Figure 2: Metamorphosis based indirect-matching of template in (a) against data in (c), which represents 2D ray transform of target in (b) (100 uniformly distributed angles in $[0, \pi]$). The second row (d)–(h) shows the image trajectory $t \mapsto \mathcal{W}(\varphi_{0,t}^\nu, f_t(\boldsymbol{\nu}, \zeta))$, so the final registered template is in (h). The third row (i)–(m) shows the deformation trajectory $t \mapsto \mathcal{W}(\varphi_{0,t}^\nu, I_0)$, likewise the fourth row (n)–(r) shows the intensity trajectory $t \mapsto f_t(\boldsymbol{\nu}, \zeta)$.

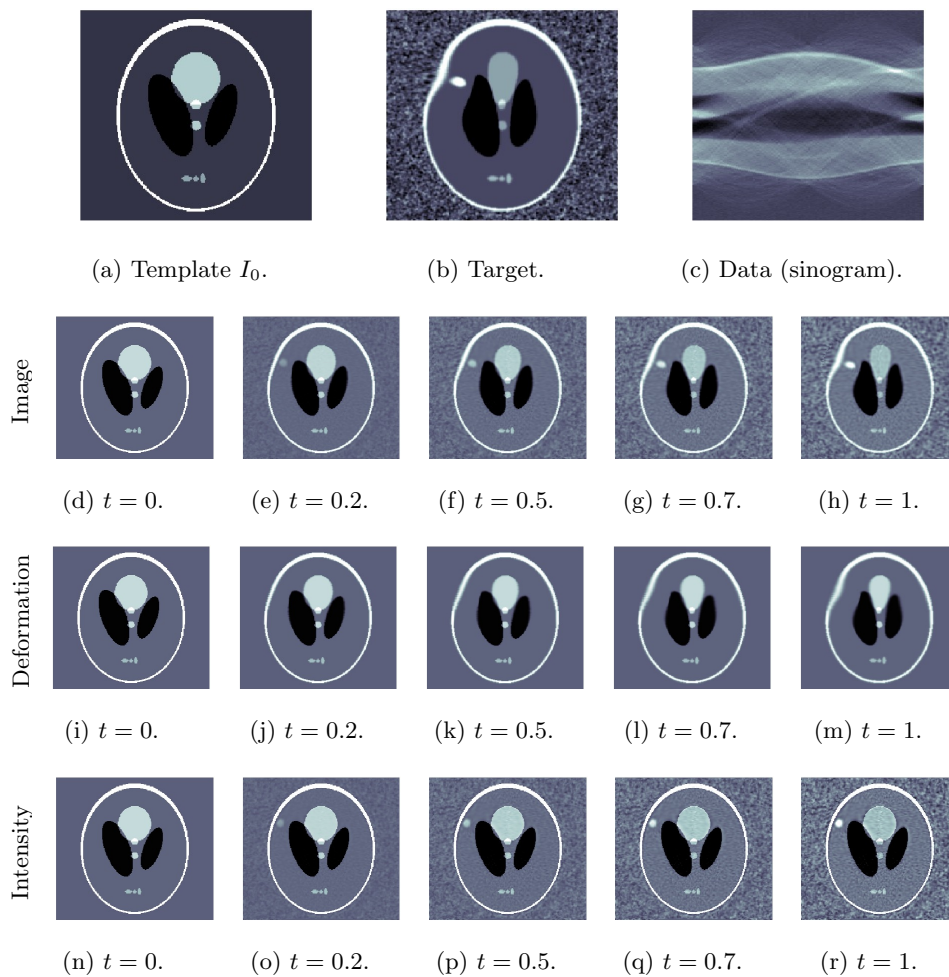


Figure 3: Metamorphosis based indirect-matching of template in (a) against data in (c), which represents 2D ray transform of target in (b) (100 uniformly distributed angles in $[0, \pi]$). The second row (d)–(h) shows the image trajectory $t \mapsto \mathcal{W}(\varphi_{0,t}^{\nu}, f_t(\nu, \zeta))$, so the final registered template is in (h). The third row (i)–(m) shows the deformation trajectory $t \mapsto \mathcal{W}(\varphi_{0,t}^{\nu}, I_0)$, likewise the fourth row (n)–(r) shows the intensity trajectory $t \mapsto f_t(\nu, \zeta)$.

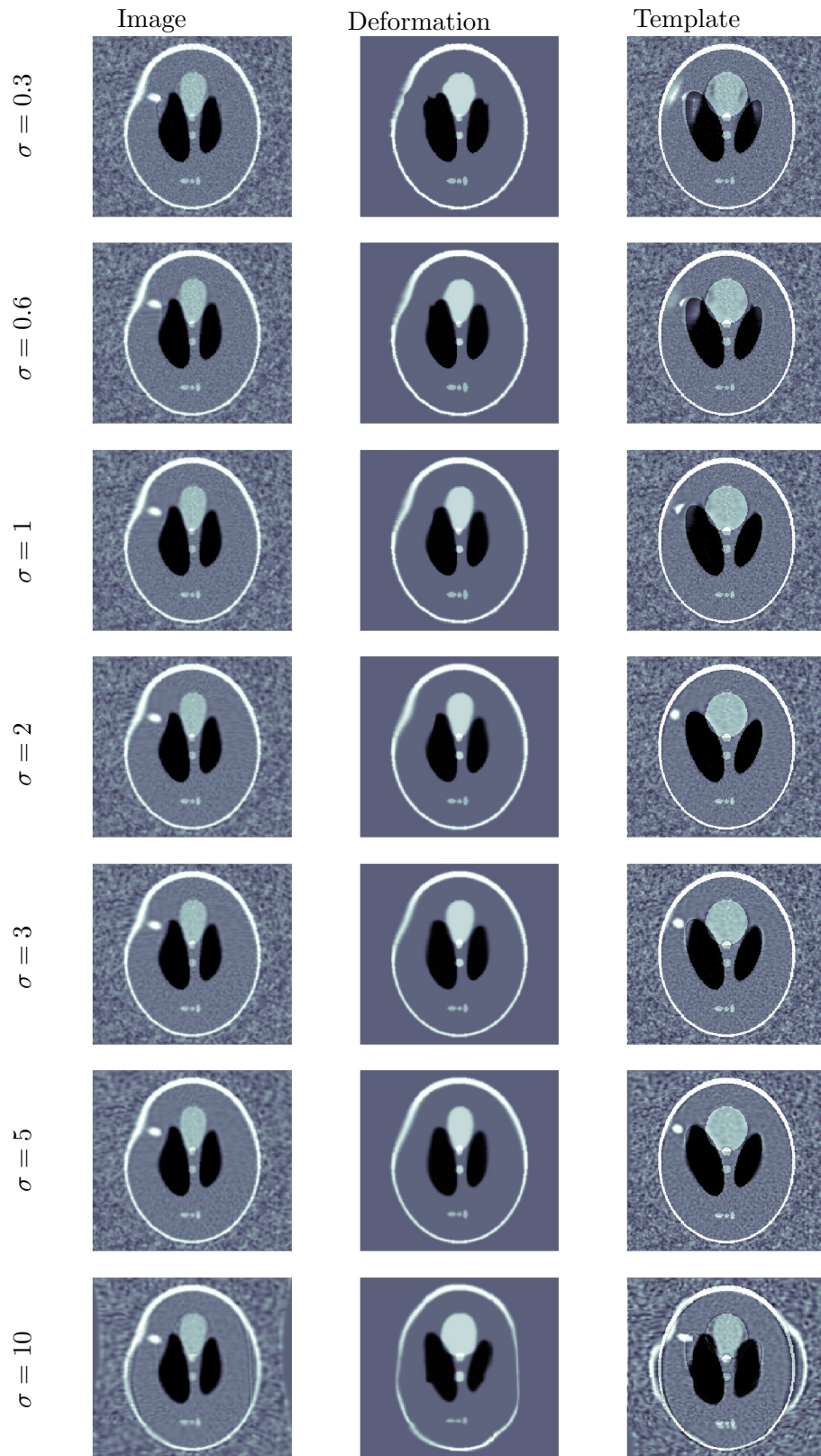
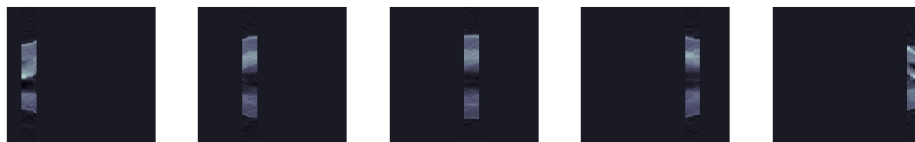


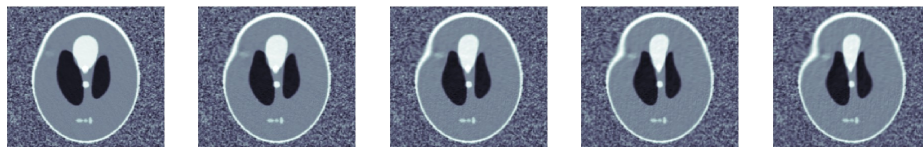
Figure 4: Reconstruction results and their recombination in template part and deformation part for various kernel size σ .



(a) The temporal evolution of the target.



(b) The (gated) tomographic data. Each data set is highly incomplete (limited angle).



(c) Image trajectory (reconstruction), combines deformation and template trajectories.



(d) Deformation trajectory, models mainly geometric changes.



(e) Template trajectory, models mainly intensity changes.



(f) FBP (left) and TV (middle) reconstructions from concatenated data (right).

Figure 5: Reconstructing the temporal evolution of a template using metamorphosis. Target (a), data (b), and results (c)–(e), are shown at selected time points $t = 0.2, 0.4, 0.6, 0.8$, and 1.0 . As a comparison we show reconstructions assuming static target obtained from concatenating the gated tomographic data (f).

A Gradient computation

This section presents the computation of the gradient of $\mathcal{J}_{\gamma,\tau}(\cdot; g)$, which is useful for any first order optimisation method for minimising the functional $\mathcal{J}_{\gamma,\tau}(\cdot; g)$ in (7). The computations assume

$$I_0 \in X \cap C^1(\Omega, \mathbb{R}) \quad \text{and} \quad (\boldsymbol{\nu}, \zeta) \in L^2([0, 1], V \times X) \quad \text{with} \quad X = L^2(\Omega, \mathbb{R}).$$

Furthermore, for each $t \in [0, 1]$ we also assume $t \mapsto \zeta(t, \cdot) \in C^1(\Omega, \mathbb{R})$. In numerical implementations, we consider digitized images and considerations of the above type are not that restrictive.

Let us first compute the differential of the data discrepancy term with respect to ζ using the notation $f_t^{\boldsymbol{\nu}, \zeta} := \mathcal{W}(\varphi_{t,0}^{\boldsymbol{\nu}}, I_t^{\boldsymbol{\nu}, \zeta}) = I_t^{\boldsymbol{\nu}, \zeta} \circ \varphi_{t,0}^{\boldsymbol{\nu}}$. As noted in (13), we have

$$f_t^{\boldsymbol{\nu}, \zeta}(x) = (I_t^{\boldsymbol{\nu}, \zeta} \circ \varphi_{t,0}^{\boldsymbol{\nu}})(x) = I_0(\varphi_{t,0}^{\boldsymbol{\nu}}(x)) + \int_0^t \zeta(\tau, \varphi_{t,\tau}^{\boldsymbol{\nu}}(x)) d\tau. \quad (27)$$

Then

$$\begin{aligned} \partial_\zeta \left[\mathcal{L}(f_t^{\boldsymbol{\nu}, \zeta}, g) \right] (\zeta)(\eta) &= \left\langle \nabla \mathcal{L}(f_t^{\boldsymbol{\nu}, \zeta}, g), \partial_\zeta f_t^{\boldsymbol{\nu}, \zeta}(\zeta)(\eta) \right\rangle \\ &= \int_\Omega \int_0^t \nabla \mathcal{L}(f_1^{\boldsymbol{\nu}, \zeta}, g) \eta(\tau, \varphi_{t,\tau}^{\boldsymbol{\nu}}(x)) d\tau dx \\ &= \int_\Omega \int_0^1 \mathbf{1}_{\tau \leq t} |\text{Det}(d\varphi_{\tau,t}^{\boldsymbol{\nu}}(x))| \nabla \mathcal{L}(f_t^{\boldsymbol{\nu}, \zeta}, g)(\varphi_{\tau,t}^{\boldsymbol{\nu}}(x)) \eta(\tau, x) d\tau dx \\ &= \left\langle \mathbf{1}_{\cdot \leq t} |\text{Det}(d\varphi_{\cdot,t}^{\boldsymbol{\nu}})| \nabla \mathcal{L}(f_t^{\boldsymbol{\nu}, \zeta}, g)(\varphi_{\cdot,t}^{\boldsymbol{\nu}}), \eta \right\rangle_{L^2([0,1], L^2(\Omega, \mathbb{R}))}. \end{aligned}$$

In order to compute the differential of the discrepancy term with respect to $\boldsymbol{\nu}$, we start by computing the differential of $f_1^{\boldsymbol{\nu}, \zeta}$ with respect to $\boldsymbol{\nu}$. Hence, let $\boldsymbol{\mu} \in L^2([0, 1], V)$ and $x \in \Omega$. Then

$$\begin{aligned} \frac{d}{d\epsilon} f_t^{\boldsymbol{\nu} + \epsilon \boldsymbol{\mu}, \zeta}(x) \Big|_{\epsilon=0} &= \left\langle \nabla I_0(\varphi_{t,0}^{\boldsymbol{\nu}}(x)), \frac{d}{d\epsilon} \varphi_{t,0}^{\boldsymbol{\nu} + \epsilon \boldsymbol{\mu}}(x) \Big|_{\epsilon=0} \right\rangle \\ &\quad + \int_0^t \left\langle \nabla \zeta(\tau, \varphi_{t,\tau}^{\boldsymbol{\nu}}(x)), \frac{d}{d\epsilon} \varphi_{t,\tau}^{\boldsymbol{\nu} + \epsilon \boldsymbol{\mu}}(x) \Big|_{\epsilon=0} \right\rangle d\tau \\ &= - \int_0^t \left\langle \nabla I_0(\varphi_{t,0}^{\boldsymbol{\nu}}(x)), d\varphi_{s,0}^{\boldsymbol{\nu}}(\varphi_{t,s}^{\boldsymbol{\nu}}(x)) \left(\boldsymbol{\mu}(s, \varphi_{t,s}^{\boldsymbol{\nu}}(x)) \right) \right\rangle ds \\ &\quad - \int_0^t \left\langle \nabla \zeta(\tau, \varphi_{t,\tau}^{\boldsymbol{\nu}}(x)), \int_t^\tau d\varphi_{s,\tau}^{\boldsymbol{\nu}}(\varphi_{t,s}^{\boldsymbol{\nu}}(x)) \left(\boldsymbol{\mu}(s, \varphi_{t,s}^{\boldsymbol{\nu}}(x)) \right) ds \right\rangle d\tau \\ &= - \int_0^t \left\langle \nabla I_0(\varphi_{t,0}^{\boldsymbol{\nu}}(x)), d\varphi_{s,0}^{\boldsymbol{\nu}}(\varphi_{t,s}^{\boldsymbol{\nu}}(x)) \left(\boldsymbol{\mu}(s, \varphi_{t,s}^{\boldsymbol{\nu}}(x)) \right) \right\rangle ds \\ &\quad - \int_0^t \int_0^s \left\langle \nabla \zeta(\tau, \cdot) \circ \varphi_{t,\tau}^{\boldsymbol{\nu}}(x), d\varphi_{s,\tau}^{\boldsymbol{\nu}}(\varphi_{t,s}^{\boldsymbol{\nu}}(x)) \left(\boldsymbol{\mu}(s, \varphi_{t,s}^{\boldsymbol{\nu}}(x)) \right) \right\rangle d\tau ds. \end{aligned} \quad (28)$$

Using (28), we can compute the derivative of $\epsilon \mapsto \mathcal{L}(\mathcal{W}(\varphi_t^{\nu+\epsilon\mu}, I_t^{\nu+\epsilon\mu, \zeta}))$ at $\epsilon = 0$:

$$\begin{aligned}
& \frac{d}{d\epsilon} \mathcal{L}(\mathcal{W}(\varphi_t^{\nu+\epsilon\mu}, I_t^{\nu+\epsilon\mu, \zeta}))|_{\epsilon=0} = \left\langle \nabla \mathcal{L}(f_t^{\nu, \zeta}, g), \frac{d}{d\epsilon} f_t^{\nu+\epsilon\mu, \zeta}|_{\epsilon=0} \right\rangle \\
& = - \int_{\Omega} \left\{ \int_0^t \nabla \mathcal{L}(f_t^{\nu, \zeta}, g)(x) \cdot \left[\left\langle \nabla I_0(\varphi_{t,0}^{\nu}(x)), d\varphi_{s,0}^{\nu}(\varphi_{t,s}^{\nu}(x))(\boldsymbol{\mu}(s, \varphi_{t,s}^{\nu}(x))) \right\rangle \right. \right. \\
& \quad \left. \left. + \int_0^s \left\langle \nabla \zeta(\tau, \cdot) \circ \varphi_{t,\tau}^{\nu}(x), d\varphi_{s,\tau}^{\nu}(\varphi_{t,s}^{\nu}(x))(\boldsymbol{\mu}(s, \varphi_{t,s}^{\nu}(x))) \right\rangle d\tau \right] ds \right\} dx \\
& = - \int_{\Omega} \left\{ \int_0^t \left| \text{Det}(d\varphi_{s,t}^{\nu}(x)) \right| \nabla \mathcal{L}(f_t^{\nu, \zeta}, g)(\varphi_{s,t}^{\nu}(x)) \cdot \right. \\
& \quad \left[\left\langle \nabla I_0(\varphi_{s,0}^{\nu}(x)), d\varphi_{s,0}^{\nu}(x)(\boldsymbol{\mu}(s, x)) \right\rangle \right. \\
& \quad \left. \left. + \int_0^s \left\langle \nabla \zeta(\tau, \cdot) \circ \varphi_{s,\tau}^{\nu}(x), d\varphi_{s,\tau}^{\nu}(x)(\boldsymbol{\mu}(s, x)) \right\rangle d\tau \right] ds \right\} dx \\
& = - \int_{\Omega} \int_0^t \left| \text{Det}(d\varphi_{s,t}^{\nu}(x)) \right| \nabla \mathcal{L}(f_t^{\nu, \zeta}, g)(\varphi_{s,t}^{\nu}(x)) \cdot \left[\left\langle \nabla(I_0 \circ \varphi_{s,0}^{\nu})(x), \boldsymbol{\mu}(s, x) \right\rangle \right. \\
& \quad \left. + \int_0^s \left\langle \nabla(\zeta(\tau, \cdot) \circ \varphi_{s,\tau}^{\nu})(x), \boldsymbol{\mu}(s, x) \right\rangle d\tau \right] ds dx \\
& = - \int_{\Omega} \int_0^1 \left\langle 1_{s \leq t} \left| \text{Det}(d\varphi_{s,t}^{\nu}(x)) \right| \nabla \mathcal{L}(f_t^{\nu, \zeta}, g)(\varphi_{s,t}^{\nu}(x)) \right. \\
& \quad \left[\nabla(I_0 \circ \varphi_{s,0}^{\nu})(x) + \int_0^s \nabla(\zeta(\tau, \cdot) \circ \varphi_{s,\tau}^{\nu})(x) d\tau \right], \boldsymbol{\mu}(s, x) \rangle ds dx \\
& = - \left\langle 1_{\cdot \leq t} \left| \text{Det}(d\varphi_{\cdot, t}^{\nu}) \right| \nabla \mathcal{L}(f_t^{\nu, \zeta}, g) \circ \varphi_{\cdot, t}^{\nu} \right. \\
& \quad \left[\nabla(I_0 \circ \varphi_{\cdot, 0}^{\nu})(\cdot) + \int_0^{\cdot} \nabla(\zeta(\tau, \cdot) \circ \varphi_{\cdot, \tau}^{\nu})(\cdot) d\tau \right], \boldsymbol{\mu} \rangle_{L^2([0,1], L^2(\Omega, \mathbb{R}^d))} \\
& = - \left\langle \int_{\Omega} K(x, \cdot) 1_{\cdot \leq t} \left| \text{Det}(d\varphi_{\cdot, t}^{\nu}(x)) \right| \nabla \mathcal{L}(f_t^{\nu, \zeta}, g)(\varphi_{\cdot, t}^{\nu}(x)) \right. \\
& \quad \left[\nabla(I_0 \circ \varphi_{\cdot, 0}^{\nu})(x) + \int_0^{\cdot} \nabla(\zeta(\tau, \cdot) \circ \varphi_{\cdot, \tau}^{\nu})(x) d\tau \right], \boldsymbol{\mu} \rangle_{L^2([0,1], V)}.
\end{aligned}$$

References

- [1] S. Arguillere, E. Trélat, A. Trouvé, and L. Younes. Shape deformation analysis from the optimal control viewpoint. *Journal de Mathématiques Pures et Appliquées*, 104(1):139–178, 2015.

- [2] M. Bauer, M. Bruveris, and P. W. Michor. Overview of the geometries of shape spaces and diffeomorphism groups. *Journal of Mathematical Imaging and Vision*, 50(1–2):60–97, 2014.
- [3] M. F. Beg, M. I. Miller, A. Trouvé, and L. Younes. Computing large deformation metric mappings via geodesic flows of diffeomorphisms. *International journal of computer vision*, 61(2):139–157, 2005.
- [4] M. Bertero, H. Lantéri, and L. Zanni. Iterative image reconstruction: a point of view. In Y. Censor, M. Jiang, and A. K. Louis, editors, *Proceedings of the Interdisciplinary Workshop on Mathematical Methods in Biomedical Imaging and Intensity-Modulated Radiation (IMRT), Pisa, Italy*, pages 37–63, 2008.
- [5] E. Bladt, D. M. Pelt, S. Bals, and K. J. Batenburg. Electron tomography based on highly limited data using a neural network reconstruction technique. *Ultramicroscopy*, 158:81–88, 2015.
- [6] M. Bruveris and D. D. Holm. Geometry of image registration: The diffeomorphism group and momentum maps. In D. E. Chang, D. D. Holm, G. Patrick, and T. Ratiu, editors, *Geometry, Mechanics, and Dynamics*, pages 19–56. Springer, 2015.
- [7] M. Bruveris, L. Risser, and F.-X. Vialard. Mixture of kernels and iterated semidirect product of diffeomorphisms groups. *Multiscale Modeling & Simulation*, 10(4):1344–1368, 2012.
- [8] N. Charon, B. Charlier, and A. Trouvé. Metamorphoses of functional shapes in Sobolev spaces. *Foundations of Computational Mathematics*, pages 1–62, 2016.
- [9] C. Chen and O. Öktem. Indirect image registration with large diffeomorphic deformations. *SIAM Journal of Imaging Sciences*, 11(1):575–617, 2018.
- [10] S. Durrleman, M. Prastawa, N. Charon, J. R. Korenberg, S. Joshi, G. Gerig, and A. Trouvé. Morphometry of anatomical shape complexes with dense deformations and sparse parameters. *NeuroImage*, 101:35–49, 2014.
- [11] A. Effland, M. Rumpf, and F. Schäfer. Image extrapolation for the time discrete metamorphosis model: Existence and applications. *SIAM Journal of Imaging Sciences*, 11(1):834–862, 2018.
- [12] M. Grasmair. Generalized Bregman distances and convergence rates for non-convex regularization methods. *Inverse Problems*, 26(11):115014, 2010.

- [13] G. T. Gullberg, B. W. Reutter, A. Sitek, J. S. Maltz, and T. F. Budinger. Dynamic single photon emission computed tomography – basic principles and cardiac applications. *Physics in Medicine and Biology*, 55:R111–R191, 2010.
- [14] J. Hinkle, M. Szegedi, B. Wang, B. Salter, and S. Joshi. 4D CT image reconstruction with diffeomorphic motion model. *Medical image analysis*, 16(6):1307–1316, 2012.
- [15] A. Markoe. *Analytic Tomography*, volume 106 of *Encyclopedia of mathematics and its applications*. Cambridge University Press, 2006.
- [16] M. I. Miller, L. Younes, and A. Trouvé. Diffeomorphometry and geodesic positioning systems for human anatomy. *Technology*, 2(1), 2014.
- [17] F. Natterer and F. Wübbeling. *Mathematical Methods in Image Reconstruction*. Mathematical Modeling and Computation. Society for Industrial and Applied Mathematics, 2001.
- [18] S. Neumayer, J. Persch, and G. Steidl. Regularization of inverse problems via time discrete geodesics in image spaces. *arXiv preprint arXiv:1805.06362*, 2018.
- [19] O. Öktem, C. Chen, N. O. Domaniç, P. Ravikumar, and C. Bajaj. Shape based image reconstruction using linearised deformations. *Inverse Problems*, 33(3):035004, 2017.
- [20] L. Risser, F.-X. Vialard, R. Wolz, M. Murgasova, D. D. Holm, and D. Rueckert. Simultaneous multi-scale registration using large deformation diffeomorphic metric mapping. *IEEE transactions on medical imaging*, 30(10):1746–1759, 2011.
- [21] A. Schwarz and M. Leach. Implications of respiratory motion for the quantification of 2D MR spectroscopic imaging data in the abdomen. *Physics in Medicine and Biology*, 45(8):2105–2116, 2000.
- [22] S. Sommer, M. Nielsen, F. Lauze, and X. Pennec. A multi-scale kernel bundle for LDDMM: towards sparse deformation description across space and scales. In *Biennial International Conference on Information Processing in Medical Imaging*, pages 624–635. Springer Verlag, 2011.
- [23] A. Sotiras, C. Davatzikos, and N. Paragios. Deformable medical image registration: A survey. *IEEE Transactions on Medical Imaging*, 32(7):1153–1190, 2013.
- [24] A. Trouvé and L. Younes. Metamorphoses through Lie group action. *Foundations of Computational Mathematics*, 5(2):173–198, 2005.

- [25] Y. Wang, E. Vidan, and G. Bergman. Cardiac motion of coronary arteries: Variability in the rest period and implications for coronary MR angiography. *Radiology*, 213(3):751—758, 1999.
- [26] L. Younes. *Shapes and Diffeomorphisms*, volume 171 of *Applied Mathematical Sciences*. Springer-Verlag, 2010.